# Theoretical study of the simplest Xe-containing molecule: HXeH

Toshiyuki Takayanagi [a,*], Tomoko Asakura [a], Kenta Takahashi [a],
Yuriko Taketsugu [b], Tetsuya Taketsugu [b], Takeshi Noro [b]

[a]*Department of Chemistry, Saitama University, 255 Shimo-Okubo, Sakura-ku, Saitama City, Saitama 338-8570, Japan*
[b]*Division of Chemistry, Graduate School of Science, Hokkaido University, Sapporo 060-0810, Japan*

## Abstract

The simplest metastable Xe-containing compound HXeH has been theoretically investigated using highly-accurate CASPT2-level electronic structure calculations taking the relativistic effects into account. A new three-dimensional global potential energy surface has been developed and time-dependent wave packet quantum dynamics calculations were then performed to obtain vibrational energy levels of the metastable states for the HXeH, HXeD and DXeD systems. It has been found that low-lying vibrational states below and just above the H + Xe + H dissociation limit have extremely long lifetimes in a nanosecond time scale. The present theoretical results suggest that these rare-gas containing molecules can experimentally be detected in the gas phase.

---

Author to whom correspondence should be addressed. Fax: +81-48-858-3700
Electronic mail: tako@chem.saitama-u.ac.jp

## 1. Introduction

Recent extensive experimental studies using a low-temperature rare-gas matrix isolation technique have clearly revealed formation of a new class of simple molecules containing rare gas atoms, H-Rg-X, where Rg is a rare gas atom and X is an electronegative atom or group [1-7]. It has been pointed out that the stability of these compounds depends on the stability of the $HRg^+$ cation and the electron affinity of X. In principle, these molecules are metastable at least in the gas phase because of the existence of the strongly exothermic pathway of $HRgX \rightarrow Rg + HX$. In addition, from extensive electronic structure calculations, upon infrared excitation, they can easily dissociate into their neutral fragments through the $HRgX \rightarrow H + Rg + X$ process in the case that the excited vibrational level of HRgX is above the H + Rg + X dissociation limit. Therefore, it should be very important to obtain accurate global potential energy surfaces in order to understand the stability and vibrational energy levels of the HRgX molecule from a theoretical point of view.

In this paper, we address the stability of the triatomic xenon dihydride HXeH since this molecule is the simplest Xe-containing molecule. The HXeH molecule was first identified in low temperature rare gas matrices by Räsänen and co-workers in 1995 [1]. They have found strong infrared absorption at 1166 $cm^{-1}$ and weak absorption at 701 $cm^{-1}$ and these absorption bands were respectively assigned to the antisymmetric stretching and bending vibrations of the neutral linear centrosymmetric HXeH molecule by comparing to ab initio molecular orbital calculations at the MP2/LANL1DZ level of theory [1]. Their assignment was further confirmed with deuterium substitution. At the same time, however, they have noticed that the energy level of the HXeH local minimum is about 2 eV higher than the energy level of the separated neutral atoms, H + Xe + H, at the MP2/LANL1DZ level. This implies that the MP2/LANL1DZ level cannot totally explain the stability of the HXeH molecule at all. Runeberg et al. [8] have performed more accurate electronic structure calculations at the MRCI and CCSD(T) levels of theory. Although they found that the HXeH minimum is more stable than the H + Xe + H dissociation limit at the MRCI level, they speculated that the

HXeH potential well cannot support the experimentally observed vibrationally excited levels. In addition, they have found that the CCSD(T) level calculations cannot give a smooth potential energy surface due to the multi-configurational character of the H + Xe + H dissociation region.

Another important aspect is the accurate theoretical prediction of vibrational spectra of HXeH by electronic structure methods. This is simply because the assignment of experimentally observed infrared absorption spectra frequently relies on theoretical results [4,9-15]. Lundell and co-workers [9] have carried out vibrational self-consistent field (VSCF) calculations for HXeH and stated that the anharmonicity for the symmetric stretching mode is important while the anharmonicity is not so important in the antisymmetric stretching and bending modes. This result seems to be reasonable since the symmetric stretching mode directly correlates to the dissociation pathway from HXeH into the neutral atomic fragments H + Xe + H. However, it should be emphasized that these results are based on the low-level MP2 calculations and that the VSCF calculations were done exclusively using the information on the force field parameters just around the HXeH potential minimum.

Motivated by the current status of theoretical studies on the HXeH molecule as mentioned above, we here present more accurate electronic structure calculations of the global potential energy surface of the $XeH_2$ system and quantum dynamics calculations for estimating accurate vibrational levels on the newly-developed potential energy surface.

## 2. Computational method

All ab initio electronic structure calculations were performed with the Molpro 2006 program [16]. We have decided to employ the multi-reference second-order perturbation theory (CASPT2) due to compromise of accuracy and computational costs. The molecular orbitals were optimized with the complete-active-space self-consistent-field (CASSCF) method, where 10 electrons (full-valence electrons)

were distributed among 9 active orbitals. These active orbitals include all valence orbitals (the 1*s* orbital of H and 5*s*5*p* orbitals of Xe) and additional three upper orbitals of Xe. In the subsequent CASPT2 calculations, the correlation effect of 4*s*, 4*p*, and 4*d* electrons of Xe was included by taking into account singles and doubles from those core orbitals to external orbitals. We have found that the electron correlation of these core electrons plays a very important role in the relative stability of HXeH with respect to the H + Xe + H dissociation level. The relativistic effects were included using the third order Douglas-Kroll relativistic one-electron integral prescription [17,18].

For Xe atom, we have employed all-electron relativistic basis sets developed by Tsuchiya et al. [19] for the inner and valence shells, which are augmented by the correlated sets of basis functions developed by Sekiya and co-workers [20-22]. The original Tsuchiya's basis set for Xe atom is a minimal one which is written as (23*s*19*p*12*d*)/[5*s*4*p*2*d*]. This set has been split in valence parts as (23,23,23,23,23/ 19,19,19,19/12,12) → (20,20,20,20,1,1,1/15,15,15,1,1,1,1/8,8,1,1,1,1), and then the Sekiya's correlated sets of (*d* / *f* / *g*) = (1,1/1,1/2) have been added where one redundant d function with an exponent of 0.493879 was eliminated. In addition, the correlated functions, $f(\alpha = 3.5)$ and $g(\alpha = 4.0)$, have been added to describe the electron correlation due to inner-shell 4*s*, 4*p*, and 4*d* electrons, and also *s* and *p* diffuse functions, determined by an even-tempered scheme, are added. The final form of the basis set for Xe atom is written as (20,20,20,20,1,1,1,1/15,15,15,1,1,1,1,1/8,8,1,1,1,1,1/1,1,1/2,1). For H atom, the segmented basis set of quadruple-zeta augmented by the correlated set has been applied, which is denoted as (5,1,1,1,1/1,1,1,1/1,1,1/1,1) [21,23].

Potential energy values were calculated at the grid points defined by H-Xe-H' internal coordinates, $R_{\text{H-Xe}}$, $R_{\text{Xe-H'}}$ and ∠H-Xe-H', where $R_{\text{H-Xe}}$ is the distance between H and Xe atoms. We have chosen 32 points for $R_{\text{H-Xe}}$ (also for $R_{\text{Xe-H'}}$) in the range of 1.4-8.0 Å and 11 points for the ∠H-Xe-H' angle in the range of 10-180 degrees. All calculations were performed under $C_s$ symmetry condition. These sets of grids thus give 5808 symmetry unique points. Finally, a three-dimensional cubic spline interpolation was employed to yield a global potential energy surface.

In order to obtain vibrational energy levels on the calculated potential energy

surface, we have carried out time-dependent wave packet calculations. The reaction system was described by the standard $J = 0$ Hamiltonian expressed in Jacobi coordinates, where $J$ is the total angular momentum quantum number of a triatomic system. The wave function was represented on a spatial grid in the radial coordinates ($R$, $r$) and in a Legendre basis for the angular coordinate γ. The size of the grid representation ($N_R$, $N_r$, $N_\gamma$) was set to (256, 256, 60) after convergence tests. We have set an appropriate Gaussian wave function around the HXeH minimum at $t = 0$ and the wave packet was subsequently propagated up to a total integration time of $t = 24$ ps using a well-known split-operator method with a time step of 0.12 fs. The $R$ and $r$ contributions to the kinetic energy were evaluated using the standard fast-Fourier-transform algorithm, while the discrete-variable-representation (DVR) [24] scheme was used for γ. In order to avoid unphysical reflection of the wave packet at the edge of the grid, numerically optimized complex absorbing potentials were used over the last 25% of the grids in $R$ and $r$. The state-density spectra were extracted from the Fourier transform of the autocorrelation function. As mentioned below, since the lifetimes of several low-lying vibrational states were found to be very long, a part of the wave packet still survives in the interaction region even after 24 ps propagation. Therefore, we have applied the appropriate Gaussian damping function $\exp(-t^2/\tau^2)$ to the autocorrelation function before performing the Fourier transform. This means that a part of the resonance widths are determined by this damping function not by resonance lifetime, as mentioned below. Details of our wave packet calculations are also described in Refs. 25 and 26.

## 3. Results and discussion

Fig. 1 shows the two-dimensional contour plot of the ground-state potential energy surface calculated at the CASPT2 level as a function of two H-Xe distances for four ∠H-Xe-H angles. The zero energy is defined as the H + Xe + H dissociation limit. The collinear H-Xe-H minimum is clearly seen in Fig. 1(a) and is located at $R_{HXe} = R_{XeH'} = 1.9496$ Å. The equilibrium geometry is in good agreement with previous

theoretical values obtained at the MP*n*, CCSD, CCSD(T), and MRCI levels of theory [4,8,9]. The potential minimum at the linear geometry is 0.276 eV below the atomic asymptotic limit of H + Xe + H. This energy value is quite close to the MRCI value (0.26 eV) of Runeberg et al [8]. The collinear saddle point is seen to be located at $R_{HXe} = R_{XeH'} = 2.5404$ Å with the barrier height of 0.033 eV above the H + Xe + H level. This barrier height is also found to be close to the MRCI value (0.03 eV) of Runeberg et al [8]. The harmonic vibrational frequencies for these two stationary points are summarized in Table 1 along with the results for isotopic variants.

Fig. 2 displays the potential energy curve for collinear configurations as a function of the symmetric stretching coordinate. The outer shallow minimum is due to attractive van der Waals interaction is seen at $R_{HXe} \sim 3.6$ Å. We have found that the present CASPT2 potential profile is quite similar to the previous MRCI result of Runeberg et al [8]. Also plotted in Fig. 2 is the harmonic potential energy curve whose force constant was determined from the second derivative value at the CASPT2 local minimum at $R_{XeH} = 1.9496$ Å. The comparison of these two curves clearly show that the harmonic approximation does not work well, as expected.

Fig. 3 shows the two-dimensional contour plot of the potential energy surface for T-shaped configurations as a function of two Jacobi radial coordinates of the Xe-$H_2$ system. This plot is given to show the HXeH $\rightarrow$ Xe + $H_2$ dissociation pathway. The left potential well corresponds to the HXeH local minimum while the right lower region corresponds to a more stable Xe + $H_2$ region. The result of Fig. 3 clearly demonstrates that the linear HXeH molecule is metastable with respect to the Xe + $H_2$ dissociation channel. However, we did not find the saddle point with a bent H-Xe-H structure in the HXeH $\rightarrow$ Xe + $H_2$ pathway. This behavior is very different from the HArF [27-29] and HHeF [25,30] cases, for which bent saddle point structures have been previously found. The difference may be presumably due to the symmetric nature of the HXeH molecule. It is then expected that the vibrationally excited HXeH molecule first dissociates into the atomic H + Xe + H fragments via the collinear saddle point when the excited level is beyond the dissociation limit and a part of the transient fragments goes into the Xe + $H_2$ region. Interestingly, we notice that previous ab initio MRCI

calculations of the potential energy surface for $XeF_2$ [31] show a similar behavior although the computational level employed was not so high.

Fig. 4 displays the energy spectra for the HXeH, HXeD, and DXeD systems obtained from the Fourier transform of the calculated autocorrelation functions. For example, in the case of HXeH (Fig. 4a), we can see five very sharp peaks at -0.0665, 0.0318, 0.0676, 0.0782 and 0.1953 eV of energy, where the zero energy is defined as the H + Xe + H dissociation limit. Several broad peaks can also been seen. We can easily extract the wave function for these resonance states using the standard numerical procedure and then assigned a set of vibrational quantum numbers ($v_s v_b^l v_{as}$) by looking at the density profile of the extracted wave function. Here, $v_s$, $v_b$, and $v_{as}$ are vibrational quantum numbers of symmetric stretching, bending, and antisymmetric stretching, respectively, and $l$ is the vibrational angular momentum quantum number for bending. Since we have done only $J = 0$ quantum dynamics calculations, we can obtain only $l = 0$ bending states. Typical two-dimensional contour plots for the wave functions of (000), (100), (001), and (200) vibrational states of HXeD are presented in Fig. 5. Notice that the density of the wave functions are plotted, but the nodal structures of these states are clearly seen, which facilitate unambiguous assignment of vibrational quantum numbers. Needless to say, in the case of the HXeD system, the symmetric and antisymmetric stretching modes nearly correspond to the Xe-D and Xe-H stretching modes, respectively. Table 2 lists the positions and quantum number assignments for the calculated vibrational states of HXeH, HXeD, and DXeD.

As a result, we found that the quantum number assignment was possible only when the resonance peak is very sharp. For broad resonance peaks, on the other hand, it was found that the nodal patterns were very complicated, and we were not able to obtain proper vibrational quantum numbers. From the results presented in Fig. 4, it is seen that the background level of the state density significantly increases at $E = 0.05 \sim 0.1$ eV. This is quite reasonable due to the opening of the H + Xe + H dissociation channel. Also, low-lying sharp peaks become dense going from the lighter HXeH system to heavier DXeD system. This is also an expected behavior. As mentioned before, it should be emphasized that the widths of these very sharp peaks are completely

determined by the damping function, i.e., total propagation time of the wave packet, not by the resonance lifetime. In principle, we can obtain the decay rate (lifetime) of the resonance state simply by doing the wave packet propagation for which the initial wave packet is set to the extracted resonance wave function. We have actually carried out such calculations; however, we were not able to obtain reliable lifetimes. This is simply because the total propagation time of wave packet is about 24 ps, which is too short for obtaining reliable lifetimes. Only in the case of the (000) state of HXeH, the lifetime was roughly estimated to be about 0.2 ns. This suggests that the lifetimes of the vibrational states for heavier HXeD and DXeD systems would be even much longer.

It should be important to give some comments on the accuracy of the harmonic approximation. In the case of HXeH, the harmonic vibrational frequency for symmetric stretching is calculated to be 1094 $cm^{-1}$(see Table 1), while the fundamental frequency (energy difference between (000) and (100) states) obtained from the quantum dynamics is 793 $cm^{-1}$. Thus, the effect of anharmonicity amounts 301 $cm^{-1}$ and is quite significant. Of course, this is not surprising since the symmetric stretching coordinate directly correlates to the H + Xe + H dissociation pathway, as mentioned before. On the other hand, for the antisymmetric stretching mode, the harmonic frequency is calculated to be 1302 $cm^{-1}$, which is 220 $cm^{-1}$ larger than the fundamental frequency (1082 $cm^{-1}$) obtained from the quantum dynamics calculations. In addition, in the case of bending, the difference between the harmonic frequency and the quantum fundamental frequency is roughly estimated to be about 100 $cm^{-1}$ although a more accurate estimate requires $J > 0$ quantum dynamics calculations in order to obtain the energy level of the ($01^{1}0$) state. All these results suggest that it may be sometimes dangerous that the harmonic vibrational frequencies obtained from ab initio electronic structure calculations are employed to assign the experimentally observed infrared absorption peaks at least for the H-Rg-X type molecule trapped in the potential well slightly below the H + Rg + X dissociation limit. However, we note that most of previous experiments on HRgX have been performed under low-temperature solid matrix conditions. Therefore, it should be important to develop accurate theoretical methods taking the effect of solid phase into account.

The present theoretical studies strongly suggest that it may be possible to detect the HXeH molecule and its isotopic variants even in the gas phase since the lifetimes of these molecules were found to extremely long (nanosecond time scale). Interestingly, Buck and co-workers [32-34] have recently succeeded in indirectly identifying the H-Xe-X (X = Cl, Br, I) molecule in the photodissociation experiments of large $Xe_n$ clusters including HX molecules in the gas phase by detecting the asymmetric distribution of the dissociating H atom fragments. In addition, they have tentatively suggested the production of the HXeH molecule in $Xe_n$ clusters [33]. We hope that the present theoretical work stimulates further experimental studies in the gas phase using more conclusive spectroscopic techniques. On the theoretical side, quantum dynamics calculations for $J > 0$ should be performed to obtain other low-lying vibrational states. Furthermore, excited-state potential energy surfaces of HXeH should be calculated in order to theoretically understand the photodissociation experiments of Buck and co-workers [33,34]. Work along this line is currently in progress in our group.

## References


[1] M. Pettersson, J. Lundell, M. Räsänen, J. Chem. Phys. 103 (1995) 205.

[2] V. I. Feldman, F. F. Sukhov, Chem. Phys. Lett. 255 (1996) 425.

[3] V. I. Feldman, F. F. Sukhov, A. Y. Orlov, Chem. Phys. Lett. 280 (1997) 507.

[4] M. Pettersson, J. Lundell, M. Räsänen, Eur. J. Inorg. Chem. (1999) 729.

[5] L. Khriachtchev, M. Pettersson, N. Runeberg, J. Lundell, M. Räsänen, Nature 406 (2000) 874.

[6] R. B. Gerber, Ann. Rev. Phys. Chem. 55 (2004) 55.

[7] V. I. Feldman, F. F. Sukhov, E. A. Logacheva, A. Y. Orlov, I. V. Tyulpina, D. A. Tyurin, Chem. Phys. Lett. 437 (2007) 207.

[8] N. Runeberg, M. Seth, P. Pyykkö, Chem. Phys. Lett. 246 (1995) 239.

[9] J. Lundell, G. M. Chaban, R. B. Gerber, J. Phys. Chem. A 104 (2000) 7944.

[10] J. Lundell, M. Pettersson, Phys. Chem. Chem. Phys. 1 (1999) 1691.

[11] S. Berski, J. Lundell, Z. Latajka, J. Mol. Struct. 552 (2000) 223.

[12] J. Lundell, M. Pettersson, M. Räsänen, Comp. Chem. 24 (2000) 325.

[13] J. Lundell, S. Berski, Z. Latajka, Phys. Chem. Chem. Phys. 2 (2002) 5521.

[14] J. Lundell, S. Berski, Z. Latajka, Chem. Phys. Lett. 371 (2003) 295.

[15] M. Solimannejad, L. M. Amlashi, I. Alkorta, J. Elguero, Chem. Phys. Lett. 422 (2006) 226.

[16] MOLPRO, version 2006.1, a package of ab initio programs, H.-J. Werner, P. J. Knowles, R. Lindh, F. R. Manby, M. Schütz, P. Celani, T. Korona, G. Rauhut, R. D. Amos, A. Bernhardsson, A. Berning, D. L. Cooper, M. J. O. Deegan, A. J. Dobbyn, F. Eckert, C. Hampel and G. Hetzer, A. W. Lloyd, S. J. McNicholas, W. Meyer and M. E. Mura, A. Nicklass, P. Palmieri, R. Pitzer, U. Schumann, H. Stoll, A. J. Stone, R. Tarroni and T. Thorsteinsson.

[17] N. Douglas, N. M. Kroll, Ann. Phys. 82 (1974) 89.

[18] B. A. Hess, Phys. Rev. A 33 (1986) 3742.

[19] T. Tsuchiya, M. Abe, T. Nakajima, K. Hirao, J. Chem. Phys. 115 (2001) 4463.

[20] M. Sekiya, T. Noro, Y. Osanai, T. Koga, Theor. Chem. Acc. 106 (2001) 297.

[21] T. Noro, M. Sekiya, T. Koga, Theor. Chem. Acc. 109 (2003) 85.

[22] http://setani.sci.hokudai.ac.jp/sapporo/

[23] H. Yamamoto, O. Matsuoka, Bull. Univ. Electro. Comm. 5 (1992) 23.

[24] J. C. Light, I. P. Hamilton, J. V. Lill, J. Chem. Phys. 82 (1985) 1400.

[25] T. Takayanagi, A. Wada, Chem. Phys. Lett. 352 (2002) 91.

[26] T. Takayanagi, Chem. Phys. 334 (2007) 109.

[27] N. Runeberg, M. Pettersson, L. Khriachtchev, J. Lundell, M. Räsänen, J. Chem. Phys. 114 (2001) 838.

[28] G. M. Chaban, J. Lundell, R. B. Gerber, Chem. Phys. Lett. 364 (2002) 628.

[29] H. Li, D. Xie, H. Guo, J. Chem. Phys. 120 (2004) 4273.

[30] G. M. Chaban, J. Lundell, R. B. Gerber, J. Chem. Phys. 115 (2001) 7341.

[31] C. M. Marian, M. Perić, Z. Phys. D 36 (1996) 285.

[32] R. Baumfalk, N. H. Nahler, U. Buck, J. Chem. Phys. 114 (2001) 4755.

[33] N. H. Nahler, M. Fárník, U. Buck, Chem. Phys. 301 (2004) 173.

[34] U. Buck, M. Fárník, Int. Rev. Phys. Chem. 25 (2006) 583.

Table 1. Harmonic vibrational frequencies[a] (in $cm^{-1}$) for collinear minimum and saddle point on the CASPT2 potential energy surface.

| | | | |
|---|---|---|---|
| Minimum at $R_{XeH} = R_{XeH'}$ =1.9496 Å | | | |
| | $\nu_s$ | $\nu_b$ | $\nu_{as}$ |
| H-Xe-H | 1094 | 723 | 1302 |
| H-Xe-D | 830 | 628 | 1220 |
| D-Xe-D | 775 | 516 | 929 |
| Transition state at $R_{XeH} = R_{XeH'}$ = 2.5404 Å | | | |
| | $\nu_s$ | $\nu_b$ | $\nu_{as}$ |
| H-Xe-H | 501 *i* | 677 | 648 |
| H-Xe-D | 416 *i* | 552 | 558 |
| D-Xe-D | 354 *i* | 462 | 483 |

[a]Vibrational modes: $\nu_s$ (symmetric stretching), $\nu_b$ (bending), and $\nu_{as}$ (antisymmetric stretching).

Table 2. Low-lying vibrational energy levels (in eV) and the quantum number assignment obtained from time-dependent wave packet calculations for $J = 0$, where $J$ is the total angular momentum quantum number.

| $(\nu_s\nu_b\nu_{as})$[a] | H-Xe-H | H-Xe-D | D-Xe-D |
|---|---|---|---|
| (000) | -0.06652 (0)[b] | -0.09454 (0) | -0.12496 (0) |
| (100) | 0.03180 (793) | -0.01358 (653) | -0.04818 (619) |
| (001) | 0.06762 (1082) | 0.02922 (998) | -0.02610 (797) |
| (020) | 0.07820 (1167) | 0.03514 (1046) | -0.01548 (883) |
| (200) | nf[c] | 0.05578 (1212) | 0.01948 (1165) |
| (101) | nf | nf | 0.04444 (1366) |
| (120) | nf | nf | 0.05148 (1423) |
| (002) | 0.19534 (2122) | nf | 0.07038 (1576) |
| (021) | nf | 0.15208 (1989) | 0.07844 (1641) |
| (040) | nf | nf | 0.08596 (1701) |
| (201) | nf | nf | 0.10246 (1834) |
| (102) | nf | nf | 0.13338 (2084) |

[a]Vibrational quantum number: $\nu_s$ (symmetric stretching), $\nu_b$ (bending), and $\nu_{as}$ (antisymmetric stretching). Since the vibrational angular momentum quantum number is 0 (due to $J = 0$), only even quantum number is allowed for bending vibration.

[b]Relative energies in $cm^{-1}$ measured from the lowest (000) vibrational state.

[c]Not found.

**Figure Captions**

Fig. 1 Contour plots of the CASPT2 potential energy surface as a function of the two Xe-H coordinates for four ∠H-Xe-H bent angles. Contours are spaced by 0.1 eV and the zero energy (bold-line contours) is defined as the H + Xe + H atomic dissociation limit. Solid lines are used for positive contours and dashed lines are for negative contours.

Fig. 2 One-dimensional potential energy profiles as a function of the symmetric stretching coordinate. Solid line corresponds to the CASPT2 result while dotted line to the harmonic potential whose parameters are determined from the information on the local minimum of the CASPT2 potential. Horizontal dashed lines indicate the vibrational energy levels for the HXeH system calculated from the quantum dynamics calculations (see Table 2).

Fig. 3 Contour plot of the CASPT2 potential energy surface for the T-shaped configurations for the $XeH_2$ system as a function of two Jacobi radial coordinates. Plot conventions for contour lines are exactly the same as Fig. 1.

Fig. 4 Energy spectra of the state density for (a) HXeH, (b) HXeD, and (c) DXeD systems obtained from the wave packet propagation calculations.

Fig. 5 Contour plots of (a) (000), (b) (100), (c) (001), and (d) (200) wave function densities of the HXeD molecule as a function of the $R_{XeH}$ and $R_{XeD}$ coordinates for collinear configurations.

Figure 1

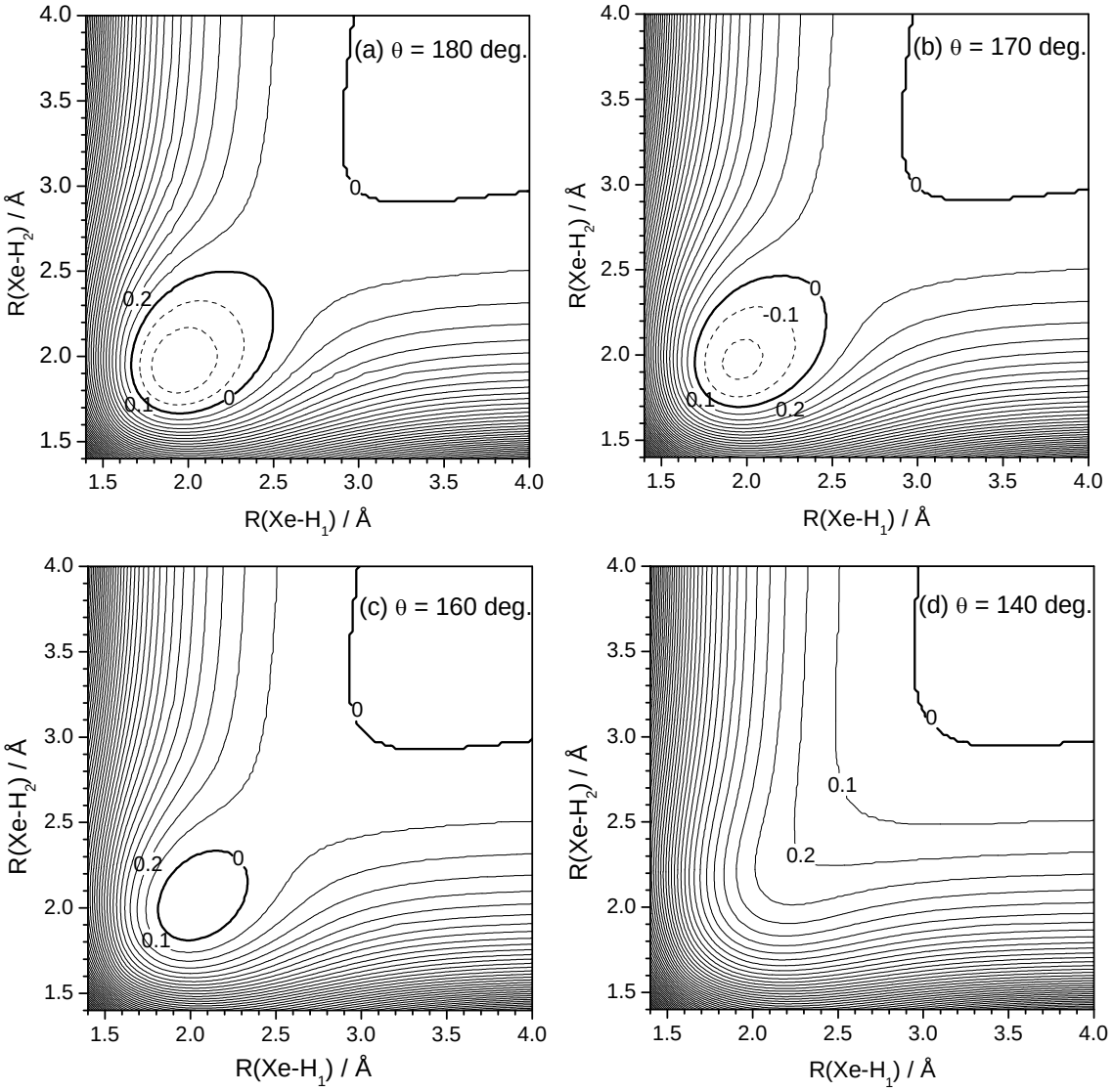
(a) θ = 180 deg.
(b) θ = 170 deg.
(c) θ = 160 deg.
(d) θ = 140 deg.
R(Xe-H2) / Å
R(Xe-H1) / Å
4.0
3.5
3.0
2.5
2.0
1.5
0
0.1
0.2
-0.1

Figure 2

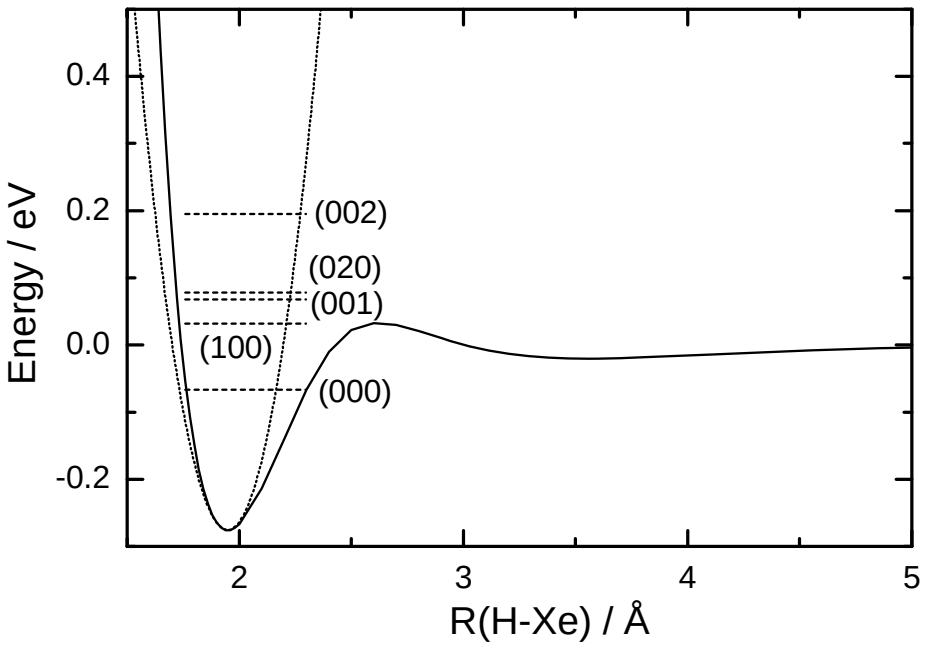

Figure 3

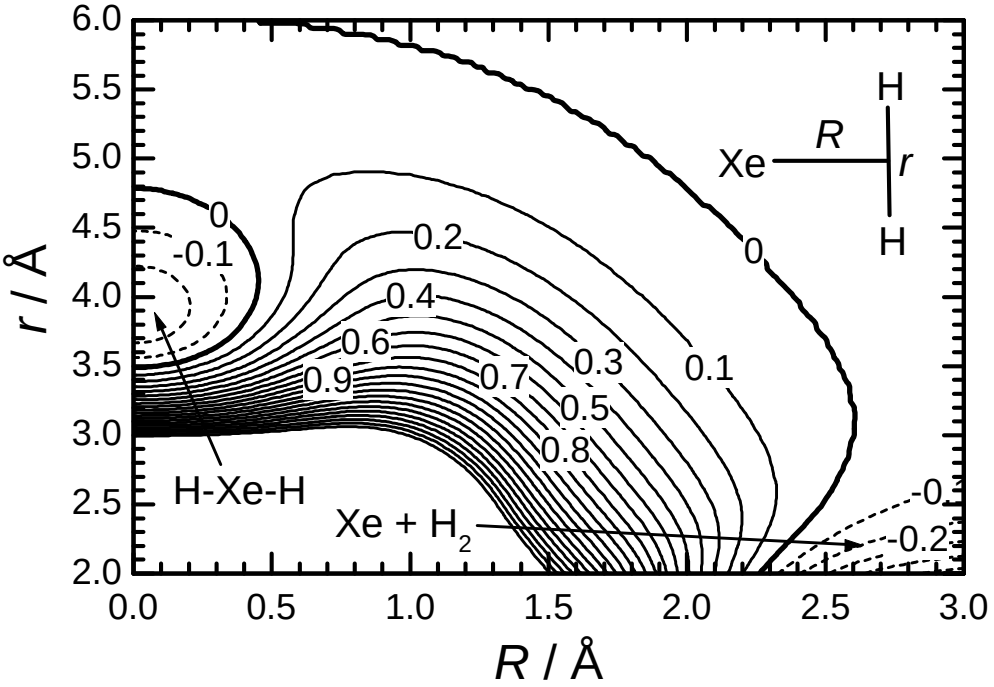
6.0
5.5
5.0
4.5
4.0
3.5
3.0
2.5
2.0
r / Å
0.0
0.5
1.0
1.5
2.0
2.5
3.0
R / Å
H
R
Xe
r
H
0
-0.1
0.2
0.4
0.6
0.9
0.7
0.3
0.1
0.5
0.8
0
-0.
-0.2
H-Xe-H
Xe + H2

Figure 4

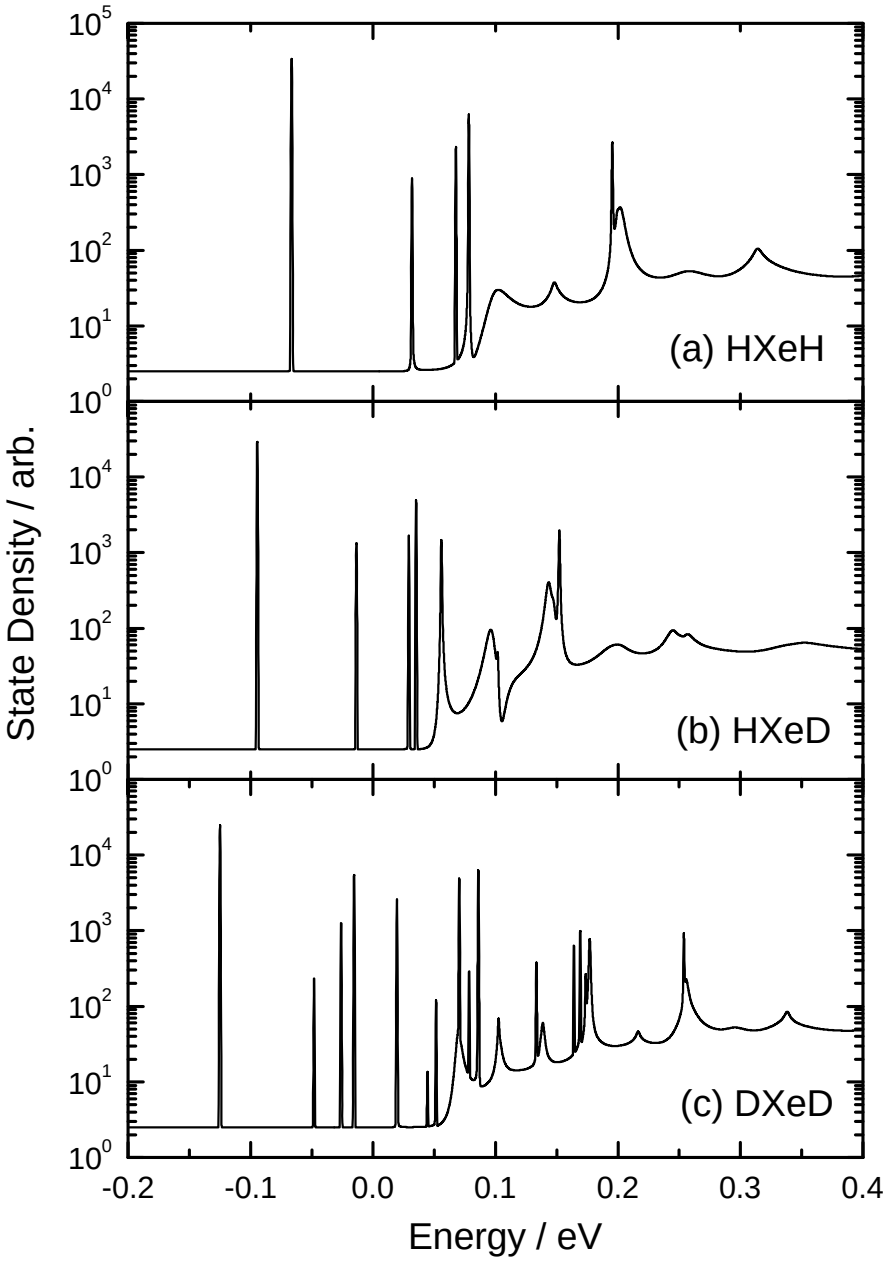
State Density / arb.
Energy / eV
(a) HXeH
(b) HXeD
(c) DXeD
$10^0$
$10^1$
$10^2$
$10^3$
$10^4$
$10^5$
-0.2
-0.1
0.0
0.1
0.2
0.3
0.4

Figure 5

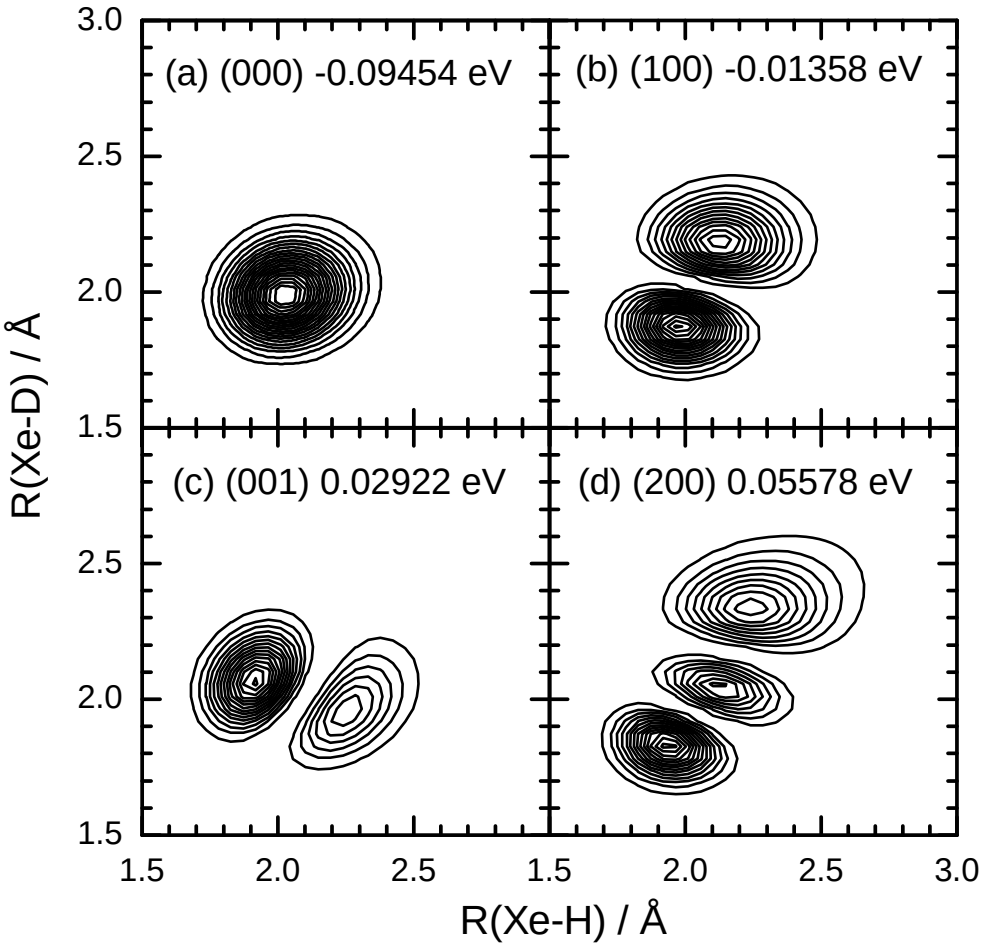
(a) (000) -0.09454 eV
(b) (100) -0.01358 eV
(c) (001) 0.02922 eV
(d) (200) 0.05578 eV
R(Xe-D) / Å
R(Xe-H) / Å
3.0
2.5
2.0
1.5
1.5
2.0
2.5
1.5
2.0
2.5
3.0